frontiers in Chemistry

ORIGINAL RESEARCH
published: 13 August 2021
doi: 10.3389/fchem.2021.734076

Assemblies of Polyacrylonitrile-Derived Photoactive Polymers as Blue and Green Light Photo-Cocatalysts for Cu-Catalyzed ATRP in Water and Organic Solvents

*Mingkang Sun, Francesca Lorandi, Rui Yuan, Sajjad Dadashi-Silab, Tomasz Kowalewski and Krzysztof Matyjaszewski**

Department of Chemistry, Carnegie Mellon University, Pittsburgh, PA, United States

Photoluminescent nanosized quasi-spherical polymeric assemblies prepared by the hydrothermal reaction of polyacrylonitrile (PAN), *ht*-PLP$_{PAN}$, were demonstrated to have the ability to photo-induce atom transfer radical polymerization (ATRP) catalyzed by low, parts per million concentrations of Cu^{II} complex with tris(2-pyridylmethyl)amine (TPMA). Such photo induced ATRP reactions of acrylate and methacrylate monomers were performed in water or organic solvents, using *ht*-PLP$_{PAN}$ as the photo-cocatalyst under blue or green light irradiation. Mechanistic studies indicate that *ht*-PLP$_{PAN}$ helps to sustain the polymerization by facilitating the activation of alkyl bromide species by two modes: 1) green or blue light-driven photoreduction of the Cu^{II} catalyst to the activating Cu^{I} form, and 2) direct activation of dormant alkyl bromide species which occurs only under blue light. The photoreduction of the Cu^{II} complex by *ht*-PLP$_{PAN}$ was confirmed by linear sweep voltammetry performed under illumination. Analysis of the polymerization kinetics in aqueous media indicated even though Cu^{I} complexes comprised only 1–1.4% of all Cu species at equilibrium, they exhibited high activation rate constant and activated the alkyl bromide initiators five to six orders of magnitude faster than *ht*-PLP$_{PAN}$.

Keywords: ATRP, photocatalyst, polyacrylonitrile, carbon dot, luminescence, self-assembly

OPEN ACCESS

Edited by:
Joanna Pietrasik,
Lodz University of Technology, Poland

Reviewed by:
Yusuf Yagci,
Istanbul Technical University, Turkey
Ajaya Bhattarai,
Tribhuvan University, Nepal

****Correspondence:***
Krzysztof Matyjaszewski
matyjaszewski@cmu.edu

Specialty section:
This article was submitted to Polymer Chemistry, a section of the journal Frontiers in Chemistry

Received: *30 June 2021*
Accepted: *04 August 2021*
Published: *13 August 2021*

Citation:
Sun M, Lorandi F, Yuan R, Dadashi-Silab S, Kowalewski T and Matyjaszewski K (2021) Assemblies of Polyacrylonitrile-Derived Photoactive Polymers as Blue and Green Light Photo-Cocatalysts for Cu-Catalyzed ATRP in Water and Organic Solvents. Front. Chem. 9:734076. doi: 10.3389/fchem.2021.734076

INTRODUCTION

Photocatalytic reactions play a profound role in various areas of chemical research (Zhu and Wang, 2017; Melchionna and Fornasiero, 2020). As alternatives to traditionally used transition metal complexes, organic photocatalysts (OPC) have received great attention, due to their low cost, highly tunable structures and photophysical properties (Romero and Nicewicz, 2016). More recently, organic photoactive nanostructured objects (OPNO) have emerged as promising materials owing to the growing interest in combining organic chemistry and nanotechnology (Han et al., 2018; Zhang et al., 2020). OPNO can span the range from covalently bonded "carbon dots" (Sun et al., 2006) to "polymer dots" (Zhu et al., 2015a; Zhu et al., 2015b; Tao et al., 2019; Xia et al., 2019) held together *via* non-covalent interactions. The synthesis of the latter type of OPNOs often relies on the pre-assembly or self-assembly of polymeric substrates, which afford additional control over the structures and properties of OPNOs (Chen and Tseng, 2017; Jia et al., 2017). Because of the heterogeneous nature of their photoactive domains, many OPNOs absorb broadly from UV to near infrared (NIR) light,

making them promising candidates as photocatalysts, due to the tunable irradiation wavelength (Zhu et al., 2015b).

Nonetheless, two main limitations remain for OPNO-based OPCs. First, most reports only focused on reactions in organic solvents. Water-soluble photocatalysts and aqueous photochemical reactions were largely omitted. Second, reactions using long-wavelength irradiations (other than blue or UV light) were underexplored, despite the advantages of long-wavelength irradiations, such as better penetration depths (Romero and Nicewicz, 2016; Han et al., 2018). Overcoming these limitations is necessary for expanding the applications of OPNO-based OPCs, obtaining deeper understandings of the photocatalytic mechanism, and economizing the photocatalytic processes (Zhang et al., 2020).

The key to solve these challenges is advancing the synthesis of OPNOs, which is traditionally limited to a narrow selection of substrates, such as citric acid/ethylenediamine (Zhu et al., 2013), conjugated polymers (Zhao et al., 2019) etc., Recently, polyacrylonitrile (PAN) has caught the attention of many researchers. PAN has been used as a substrate in the manufacturing of carbon fibers and heteroatom-doped nanocarbons (Tang et al., 2005; Zhong et al., 2012; Kopeć et al., 2017; Gottlieb et al., 2019; Kopeć et al., 2019; Yuan et al., 2019; Yuan et al., 2020). The photoluminescent properties of PAN were largely ignored, since untreated isolated nitrile groups do not form photoactive conjugated structures. However, recent reports point out that PAN can generate photoluminescence when dissolved at high concentrations or densely grafted from flat silica surfaces (Jang et al., 2006; Zhou et al., 2016; Kopeć et al., 2020). Additionally, there are recent reports of chemical conversion of PAN into photoactive species *via* microwave (Go et al., 2017), pyrolysis (Cao et al., 2020) and hydrothermal reactions (Ermakov et al., 2000; Sun et al., 2020), which all can induce the crosslinking or the hydrolysis of -C≡N, resulting in photoluminescent crosslinked nanoparticles or polymers. In particular, we recently reported the synthesis of visible light-absorbing photoluminescent polymers (PLPs) from PAN *via* a one-step hydrothermal reaction (Sun et al., 2020). In certain solvents (e.g., water), the resulting PLPs can self-assemble into polymer dot-like OPNOs. For example, the hydrothermally synthesized photoluminescent polymer (*ht*-PLP_{PAN}) assembles in water into spherical aggregates with an average diameter of ca. 20 nm, due to the presence of both hydrophilic (i.e., carboxylic) and hydrophobic (i.e., aliphatic carbons) moieties. The assembly behavior was studied mainly by dynamic light scattering (DLS) in multiple solvents, including water and dimethyl sulfoxide (DMSO) (Sun et al., 2020). The high water solubility (>100 mg/ml) makes *ht*-PLP_{PAN} a promising candidate as an OPNO-based OPC in aqueous systems.

One of the most particularly promising photochemical processes in polymer chemistry is photoinduced controlled radical polymerization (CRP), which has emerged as a powerful and versatile method for controlled polymer syntheses (Pan et al., 2016a; Chen et al., 2016; Dadashi-Silab et al., 2016; Corrigan et al., 2020; Parkatzidis et al., 2020). Similar to other externally controlled CRP methods (Chmielarz et al., 2017; Mohapatra et al., 2017; Wang et al., 2017; Pan et al., 2018), photoinduced CRPs exhibit many advantages, such as excellent temporal control. In particular, photoinduced atom transfer radical polymerization (ATRP) (Wang and Matyjaszewski, 1995; Matyjaszewski and Xia, 2001; Matyjaszewski, 2012; Dadashi-Silab et al., 2014; Matyjaszewski and Tsarevsky, 2014; Theriot et al., 2016; Matyjaszewski, 2018; Lorandi and Matyjaszewski, 2020) and reversible addition-fragmentation chain-transfer (RAFT) polymerization (Xu et al., 2015; Pearson et al., 2016; Perrier, 2017; Allegrezza and Konkolewicz, 2021) have largely benefited from the development of OPCs, such as phenothiazine derivatives (Treat et al., 2014; Pan et al., 2016b; Theriot et al., 2016; Dadashi-Silab et al., 2021), eosin Y (Kutahya et al., 2016; El Achi et al., 2020) and halogenated xanthene dyes (Wu et al., 2019). Besides small-molecule OPCs, OPNOs have been applied in photoinduced CRP (Jiang et al., 2018; Kütahya et al., 2020; Hao et al., 2021; Kütahya et al., 2021). For example, heteroatom-doped carbon dots were applied in photoinduced energy/electron transfer RAFT (PET-RAFT) polymerization of (meth)acrylate monomers (Jiang et al., 2018). Doping S or P to the catalyst enabled successful PET-RAFT polymerization under red light. Additionally, photoinduced ATRP using low ppm (parts per million) loadings of Cu complexes was performed using carbon dots or polymer dots under blue light irradiation (Kütahya et al., 2020; Kütahya et al., 2021). In these systems, carbon dots reduced the Cu^{II} complex to the corresponding Cu^{I} complex, which activated the alkyl bromide initiator. Cu^{II} complexes functioned as deactivators to provide control over the polymerization (Kütahya et al., 2020).

Nevertheless, photoinduced CRPs in the presence of OPNOs primarily employed organic solvents and oleophilic monomers (Jiang et al., 2018; Kütahya et al., 2020; Kütahya et al., 2021). Although photoinduced CRPs in aqueous media were reported using other types of catalysts (Konkolewicz et al., 2012; Pan et al., 2015; Szczepaniak et al., 2020), extending these processes to new catalysts with different structures and photoluminescent mechanisms is needed to expand the understanding of the reaction mechanisms. Furthermore, ATRP using OPNOs under long-wavelength irradiations is underexplored compared to RAFT polymerization.

Herein, we expand the applicability of photoinduced ATRP by developing Cu-catalyzed ATRP in the presence of *ht*-PLP_{PAN} as OPCs under blue (λ_{max} = 450 nm) and green (λ_{max} = 520 nm) light irradiation. During initial attempts, *ht*-PLP_{PAN} did not initiate the polymerization when used as a photoinitiator in free radical polymerization (FRP) under inert atmosphere (N_2). Nonetheless, well-controlled polymerizations were successfully performed in water and in organic solvents (DMSO, dimethylformamide or DMF, and anisole) in the presence of alkyl bromide initiators and 25–500 ppm of Cu^{II} complexes (Br-Cu^{II}/L, L = ligand). A low loading of *ht*-PLP_{PAN} (<1 mg/ml) and moderate light intensities (4–6 $mW.cm^{-2}$) were used. Aqueous Cu-catalyzed ATRP of a water-soluble monomer, oligo (ethylene glycol) methyl ether methacrylate (OEGMA), is shown in **Scheme 1**. Studies performed under different irradiation wavelengths revealed that under blue light

irradiation *ht*-PLP_{PAN} could both reduce the Cu^{II} complexes and activate alkyl halides. In contrast, under green light irradiation it was only capable to reduce the Cu^{II} complexes.

MATERIALS AND METHODS

Materials

Methyl methacrylate (MMA, 99%, Sigma-Aldrich, United States), oligo (ethylene glycol) methyl ether methacrylate (OEGMA, average MW = 500, Sigma-Aldrich, United States), acrylonitrile (AN, 99%, Sigma-Aldrich) and methyl acrylate (MA, 99%, Sigma-Aldrich, United States) were purified by passing the monomers through a column filled with basic alumina to remove the inhibitor. Deionized water (DI water) was obtained from Millipore-Sigma Milli-Q water purification system. Azobisisobutyronitrile (AIBN, 98%, Sigma-Aldrich, United States) was recrystallized in anisole and stored at 4°C in dark. Tris (2-pyridylmethyl)amine (TPMA) was synthesized based on previously reported methods (Xia and Matyjaszewski, 1999). Copper bromide ($CuBr_2$, 99%, Acros Organics, United States), ethyl α-bromoisobutyrate (EBiB, 98%, Sigma-Aldrich, United States), ethyl α-bromophenylacetate (EBPA, 97%, Sigma-Aldrich, United States), 2-hydroxyethyl 2-bromoisobutyrate (HO-EBiB, 95%, Sigma-Aldrich, United States), 2-bromopropionitrile (BPN, 97%, Sigma-Aldrich, United States), deuterated DMSO (DMSO-d_6, 99.9%, Cambridge Isotope Laboratories, United States), deuterium oxide (D_2O, 99.9%, Cambridge Isotope Laboratories), anisole (99%, Sigma-Aldrich, United States), dimethyl sulfoxide (DMSO, 99.7%, Fisher, United States), toluene (99%, Fisher, United States), and dimethylformamide (DMF, 99.8%, Fisher, United States) were used as received. Tetraethylammonium tetrafluoroborate (Et_4NBF_4, 99%, Alfa Aesar, United States), used as a supporting electrolyte for electrochemical analysis, was recrystallized from ethanol, and dried in a vacuum oven at 70°C for 48 h.

Instruments

^1H nuclear magnetic resonance (NMR) was conducted on a Bruker 500 MHz AVANCE III NMR spectrometer. Polymerizations in organic solvents used DMSO-d_6 as the solvent for ^1H NMR, and D_2O for aqueous ATRP. DMF GPC was equipped with a refractive index (RI) detector, an Agilent 1260 Infinity II pump and a Wyatt Optilab T-rEX RI detector, with a PSS GRAM analytical column set (10 μm particle size) and LiBr-containing HPLC grade DMF as the eluent (LiBr: 0.05 M). Agilent EasiVial poly (methyl methacrylate) (PMMA) calibration kit (part number: PL 2020-0200) was used to calibrate the RI detector of GPC. Blue (λ_{max} = 450 nm, 5.0 $mW.cm^{-2}$) and green (λ_{max} = 520 nm, 4.7 $mW.cm^{-2}$) LED lights were purchased from aspectLED. The light intensity was measured by a ThorLabs PM100D compact power and energy meter console. The photoreactor for polymerization was prepared by mounting LED strips inside a round glass container, and air flow was applied to limit temperature increase during the polymerization. Solvent evaporation was performed on a Biotage V10 rapid solvent removal system. UV-vis spectra were taken on an Agilent Cary 60 UV-vis spectrometer and recorded by Cary WinUV software. Linear sweep voltammetries were measured by an Autolab PGSTAT302N potentiostat/galvanostat (Metrohm) run by a computer with NOVA 2.0 software. Dynamic light scattering (DLS) was measured by a Malvern Zetasizer Ultra light scattering system. Transmission electron microscopy (TEM) was performed using a JEOL JEM-2000EX TEM.

Synthesis of *ht*-PLP_{PAN}

ht-PLP_{PAN}, was synthesized *via* previously reported procedures (Sun et al., 2020). PAN_{165} (subscript defines the degree of polymerization) was used to prepare *ht*-PLP_{PAN} and was synthesized by initiators for continuous activator regeneration (ICAR) ATRP using BPN as the initiator (Lamson et al., 2016; Kopeć et al., 2017). In a typical procedure, a 10 mg/ml suspension of ball-milled PAN_{165} in DI water was prepared. 10 ml suspension was stirred for 10 min and then transferred to a 25 ml autoclave reactor with high-temperature resistant liner. The autoclave reactor was securely sealed and placed in a pre-heated oven (180°C). The heating was turned off after 12 h and the oven was let to cool down to room temperature naturally. The dark brown solution was passed through a 0.22 μm syringe filter with a polyethersulfone membrane. The solution was directly dried by vacuum to yield brown solid *ht*-PLP_{PAN}.

General Procedure for Light-Mediated ATRP in the Presence of *ht*-PLP_{PAN}

In a typical procedure, 5 mg *ht*-PLP_{PAN} was added to a 10 ml Schlenk flask containing 0.3 ml DMF and 7.2 ml DI water with a magnetic stir bar. HO-EBiB (3.9 μL, 0.027 mmol, 1 eq), $CuBr_2$ (0.60 mg, 2.7 μmol, 0.1 eq), TPMA (2.35 mg, 8.1 μmol, 0.3 eq), NaBr (41.17 mg, 0.4 mmol), OEGMA (2.5 ml, 5.4 mmol, 200 eq) were subsequently added to the Schlenk flask. The Schlenk flask was then purged with N_2 for approx. 25 min, and 0.1 ml of the reaction was withdrawn and was used as the "t = 0" sample. Finally, the Schlenk flask was placed in the photoreactor, and light was turned on to start the polymerization. The conversion of OEGMA was monitored by ^1H NMR by withdrawing samples (~0.1 ml each time) from the reaction mixture at different time points.

General Procedures for Voltammetric Measurements

Linear sweep voltammetries were carried out in a 5-neck electrochemical cell placed inside the photoreactor, equipped with a 3-electrode system and connected to an Autolab PGSTAT302N potentiostat/galvanostat (Metrohm) controlled by NOVA 2.0 software. The 3-electrode system was composed by: 1) a Pt foil counter electrode; 2) a homemade quasi-reference electrode: Ag|AgI|(0.1 M *n*-Bu_4NI in DMF); 3) a glassy carbon (GC) disk tip (3 mm dia, Metrohm), connected to a rotating disk electrode (RDE) system, as working electrode. Before each experiment, the GC disk was cleaned by polishing with a 0.25-μm diamond

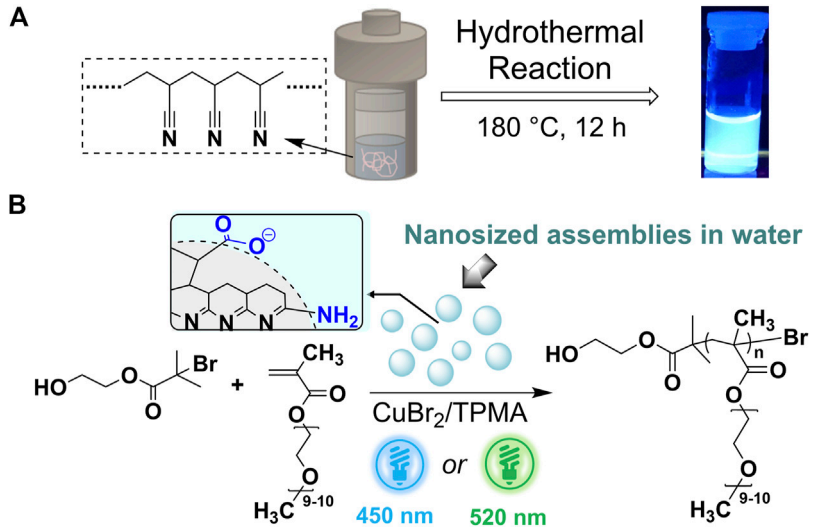

SCHEME 1 | (A) Schematic representation of the synthesis of *ht*-PLP_{PAN}, and an image of *ht*-PLP_{PAN} dissolved in water under UV light excitation (365 nm) **(B)** Proposed assembled structure of *ht*-PLP_{PAN} based on the previous report (Sun et al., 2020), and the use of *ht*-PLP_{PAN} as the photo-cocatalyst in Cu-catalyzed light-mediated ATRP. Functional groups highlighted in blue represent typical hydrophilic fragments.

paste, followed by ultrasonic rinsing in ethanol for 5 min. Ferrocene (Fc) was added at the end of each experiment as an internal standard, to refer all potentials to the saturated calomel electrode [SCE, $E^{\circ}(Fc^{+}|Fc) = 0.475$ V vs SCE in DMF]. A steady air flow was applied to limit the temperature increase caused by light irradiation, and all experiments were performed under inert atmosphere (N_2).

RESULTS AND DISCUSSION

Photophysical Properties of *ht*-PLP_{PAN}

ht-PLP_{PAN} was synthesized based on a previously reported hydrothermal reaction (Sun et al., 2020). Dynamic light scattering (DLS) measurement suggested that *ht*-PLP_{PAN} formed aggregates in water (**Supplementary Figure 1**). Transmission electron microscopy (TEM) revealed that the average diameter of the quasi-spherical assemblies was ca. 20 nm (**Supplementary Figure 2**). At first, using *ht*-PLP_{PAN} as a photoinitiator in FRP was attempted under blue or green light irradiation. However, no polymerization was observed under N_2 atmosphere in the absence of additional initiators (**Table 1**, entries 5 and 9, discussed in detail later). Thus, our focus shifted to using *ht*-PLP_{PAN} as a reducing agent for the $CuBr_2$ complex with a common ATRP ligand, tris(2-pyridylmethyl) amine (TPMA). (Xia and Matyjaszewski, 1999).

To evaluate the capability of *ht*-PLP_{PAN} in photoreducing the $CuBr_2$/TPMA complex, photophysical properties of *ht*-PLP_{PAN} (**Figure 1**) were analyzed. Our previous study reported a broad UV-vis absorption profile (**Figure 1A**) and a short lifetime of the excited state *ht*-PLP_{PAN} (<5 ns), suggesting the singlet nature (Sun et al., 2020). Putative photophysical properties of *ht*-PLP_{PAN} were modeled using density functional theory (DFT) calculations with model oligoimine-based structures of different conjugation lengths oI_N (where N = 3–10 denotes the number of nitrogen atoms along the backbone), which were deemed likely to arise in the course of hydrothermal treatment (**Figure 1B**, see **Supplementary Material** for Cartesian coordinates). (Sun et al., 2020) In all instances, the energies of the lowest unoccupied molecular orbital (LUMO) of oI_N were higher than the LUMO (β) of $[Br\text{-}Cu^{II}/TPMA]^{+}$, indicating conditions favorable for reduction of the Cu^{II} complex upon photoexcitation (**Figure 1C**). The $LUMO_{oIN}$-$LUMO_{[Br\text{-}Cu^{II}/TPMA]^{+}}$ gap increased, and the wavelength of the lowest-energy transition determined by time-dependent DFT (TDDFT) decreased with the decrease of N (**Supplementary Figure 3**), suggesting stronger "reducing power" of blue light absorbing species, in agreement with experimental observations. Experimental studies on the photoreduction of the Cu^{II} complex were performed using linear sweep voltammetry (LSV), which are discussed in *Photocatalytic Mechanism and Comparison Between Activation by Cu^{I} Complex and by ht-PLP_{PAN}* section.

Cu-Catalyzed ATRP in Water Using *ht*-PLP_{PAN}

Blue (λ_{max} = 450 nm) and green light sources (λ_{max} = 520 nm) were chosen for photoinduced ATRP using *ht*-PLP_{PAN}. Oligo (ethylene glycol) methyl ether methacrylate with an average molecular weight of 500 ($OEGMA_{500}$) was polymerized using ATRP catalyzed by a $CuBr_2$-complex with TPMA as the ligand (molar ratio: $CuBr_2$/TPMA = 1/3) (**Table 1**). 100 ppm or 500 ppm (relative to the monomer concentration) of $CuBr_2$/TPMA were used, with 2-hydroxyethyl 2-bromoisobutyrate (HO-EBiB) as the ATRP initiator and 0.5 mg/ml *ht*-PLP_{PAN} as the photo-cocatalyst. Additionally, 40 mM of NaBr was added to suppress the dissociation of the weak Cu^{II}-Br bond in the ATRP deactivator (Simakova et al., 2012; Fu et al., 2018).

TABLE 1 | Cu-catalyzed photoinduced ATRP of $OEGMA_{500}$ in water[a] with HO-EBiB as the initiator and *ht*-PLP_{PAN} as the photo-cocatalyst (0.5 mg/ml).

Entry	Irradiation	$[M]_0/[I]_0/[CuBr_2]_0/[TPMA]_0$	Conv. (%)	$M_{n,theo}$[b]	$M_{n,GPC}$[c]	$Đ$
1	Blue (450 nm)[d]	200/1/0.1/0.3	98 (2.5 h)	98,300	50,700	1.35
2		200/1/0.02/0.06	92 (3 h)	92,000	72,600	1.69
3		200/1/0.02/0.06 (no *ht*-PLP_{PAN})	<5 (8 h)	–	–[e]	–
4		200/1/0/0	56 (8 h)	56,400	413,000	2.74
5		200/0/0/0	<5 (12 h)	–	–	–
6	Green (520 nm)[f]	200/1/0.1/0.3	87 (5 h)	87,700	49,100	1.38
7		200/1/0.02/0.06	81 (12 h)	81,900	62,200	1.55
8		200/1/0/0	<5 (48 h)	–	–	–
9		200/0/0/0	<5 (20 h)	–	–	–

[a]*General conditions: Vol%(OEGMA) = 25%, and H_2O (containing 40 mM NaBr and 3 vol% of DMF as internal standards for ^1H NMR) was used as the solvent.*
[b]*$M_{n,theo}$ was determined by the monomer conversion monitored by ^1H NMR.*
[c]*$M_{n,GPC}$ was calculated from a linear PMMA calibration.*
[d]*Intensity: 5.0 mW cm^{-2}.*
[e]*No polymer signal was observed from GPC.*
[f]*Intensity: 4.7 mW cm^{-2}.*

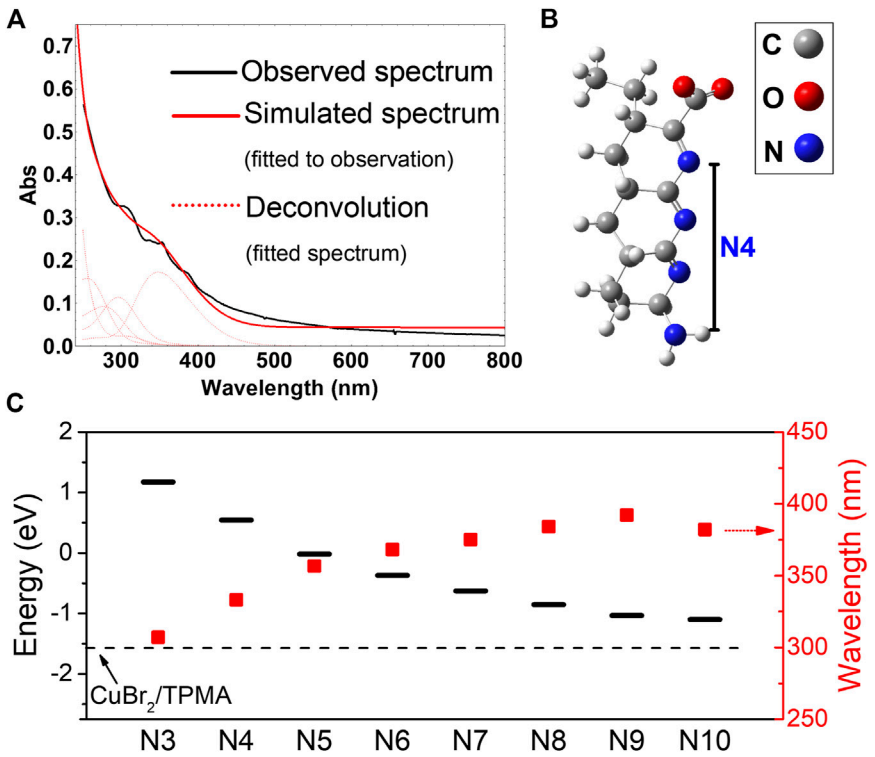

FIGURE 1 | Photophysical properties of *ht*-PLP_{PAN} **(A)** Experimental and simulated UV-vis spectra of *ht*-PLP_{PAN} calculated by time-dependent density functional theory (TDDFT). Structure optimization and TDDFT calculations were performed in simulated water environment using a polarizable continuum model, at the ωB97X-D/6-31g-d and cam-b3lyp/6-31g-d levels, respectively **(B)** A representative model structure for photoactive domains of *ht*-PLP_{PAN} with four nitrogen atoms (oI_4), optimized at the ωB97X-D/6-31g-d level (Stephens et al., 1994; Frisch et al., 2016). **(C)** Energy levels of the lowest unoccupied molecular orbital (LUMO, black bars) and wavelengths of the lowest energy transition (red squares) of model structures (oI_3 to oI_{10}) with different conjugation lengths represented by the number of nitrogen atoms within the backbone (Sun et al., 2020). The dashed line represents the energy of the LUMO (β) of the $[Br\text{-}Cu^{II}/TPMA]^+$ complex in water [optimized at the ωB97X-D level with def2TZVP basis set on Cu and 6-31g-d basis set on the other atoms (Miertuš and Tomasi, 1981; Chai and Head-Gordon, 2008)].

First, polymerizations were performed under blue light irradiation. Linear semilogarithmic kinetic plots for ATRP using both 500 ppm (entry 1, **Table 1**) and 100 ppm (entry 2, **Table 1**) of the Cu^{II} complex are shown in **Figure 2A**. Polymer molecular weight and dispersity ($Đ$) were measured by gel permeation chromatography (GPC) using dimethylformamide (DMF) as the mobile phase (**Figure 2B**). Increasing the loading of $CuBr_2$/TPMA from 100 ppm (entry 2) to 500 ppm (entry 1) resulted in a decreased $Đ$ from 1.69 (entry 2) to 1.35 (entry 1), due to the higher equilibrium concentration of the deactivator.

Clean shifts of the molecular weight distribution (MWD) traces are shown in **Supplementary Figure 4**. It is worth mentioning that the difference in the molecular weight measured from the light scattering (LS) detector of GPC ($M_{n,GPC}$) and the theoretical molecular weight ($M_{n,theo}$) was likely due to different polymer-column interactions between poly (OEGMA) and the calibration standard (PMMA) used for the calibration of the LS detector. **Figure 2A** also illustrates that the rate of polymerization for entry 1 (500 ppm of Cu complex) was faster than that for entry 2 (100 ppm of Cu complex). This difference was attributed to the higher concentration of propagating radicals in entry 1 and faster reduction of the Cu^{II} complex. Similar kinetic results were previously reported by several ATRP methods based on activator regeneration (Simakova et al., 2012; Mendonça et al., 2014). Despite the lower monomer conversion determined by ^1H NMR, entry 2 showed a higher $M_{n,GPC}$ than entry 1 (**Table 1**). This difference indicated that the initiation efficiency of HO-EBiB was lower when a lower loading of $CuBr_2$/TPMA was used in entry 1.

In order to confirm the role of *ht*-PLP_{PAN}, a control experiment was performed in its absence (entry 3, **Table 1**). No substantial monomer conversion (<5% after 8 h) was observed, indicating that the *ht*-PLP_{PAN} was required to generate the Cu^I activator complex. In addition, the possibility of direct activation of the alkyl bromide (R-Br) initiator by *ht*-PLP_{PAN} was considered. A control experiment (entry 4, **Table 1**) showed that under blue light irradiation HO-EBiB was indeed activated in the presence of *ht*-PLP_{PAN} and in the absence of the Cu^{II} complex. The polymerization was uncontrolled ($Đ$ = 2.74) due to the absence of Cu^{II} deactivators. In comparison, no polymerization occurred when no HO-EBiB was added, indicating that *ht*-PLP_{PAN} did not generate radicals directly from the monomer. A quantitative comparison between the activation of R-Br by the Cu^I complex and by *ht*-PLP_{PAN} is presented in the *Photocatalytic Mechanism* section.

Similar polymerizations were conducted under green light irradiation (entries 6–7, **Table 1** and **Figure 2**). In general, polymerization rates under green light irradiation were slower than those under blue light irradiation, and proceeded only after an induction period (**Figure 2A**). Finally, similar control experiments (entries 8 and 9, **Table 1**) were performed under green light. In contrast with the control experiments performed under blue light, no polymerization was observed under green light irradiation in the absence of Cu^{II}, indicating that *ht*-PLP_{PAN} luminophores excited by this range of wavelengths were not capable to activate the alkyl bromide initiator under green light, even after prolonged irradiation (48 h, entry 8, **Table 1**).

In addition to the already discussed lower "reducing power" of longer-wavelength luminophores inferred from DFT model calculations, two other factors that could be responsible for the slower polymerization and absence of *ht*-PLP_{PAN}-driven activation of R-Br under green light are: 1) the lower light absorption of *ht*-PLP_{PAN} at 520 nm (**Figure 1**), and 2) the slightly lower intensity of the green light photoreactor (4.7 $mW.cm^{-2}$, vs 5.0 $mW.cm^{-2}$ of the blue light photoreactor). Nevertheless, green light irradiation still resulted in reasonably well-controlled polymerization of $OEGMA_{500}$ ($Đ$ = 1.38) using 500 ppm of Cu^{II}/TPMA (entry 6, **Table 1**).

Cu-Catalyzed ATRP in Organic Solvents Using *ht*-PLP_{PAN}

To demonstrate the versatility of *ht*-PLP_{PAN} as OPCs, a mixed solvent containing 1:1 (v/v) of DMSO and DMF was first used to polymerize MMA with ethyl α-bromophenylacetate (EBPA) as the initiator. It is worth mentioning that *ht*-PLP_{PAN} only partially dissolved when using DMSO/DMF due to the lower polarity of the reaction media, especially after the addition of MMA. Despite the weaker solubility of *ht*-PLP_{PAN}, well-controlled polymerizations were obtained with *ht*-PLP_{PAN} dispersed in the solvent using 100 ppm or 25 ppm of $CuBr_2$/TPMA as the catalyst (**Table 2**).

Similar to the case of aqueous media, better control was obtained for the polymerization of MMA with a higher loading of $CuBr_2$/TPMA (entries 1 and 5, **Table 2**). However, 500 ppm of the Cu complex were required to control the process in aqueous media (entries 1 and 6, **Table 1**), while concentrations of Cu^{II} complex as low as 25 ppm were sufficient in organic solvents (entry 6, **Table 2**). Linear semilogarithmic kinetic plots and the GPC traces observed under those conditions are shown in **Figure 3**. Clean shifts of GPC traces were also observed (**Supplementary Figure 5**). Additionally, the direct activation of EBPA by *ht*-PLP_{PAN} was evaluated by control experiments in the absence of $CuBr_2$/TPMA (entries 3 and 7, **Table 1**). Similar to results in aqueous media, *ht*-PLP_{PAN} activated EBPA only under blue light irradiation. The supplemental activation of EBPA under blue light irradiation likely contributed to the higher dispersity when 25 ppm loading of $CuBr_2$/TPMA was used (entry 2). The uncontrolled polymerization in the absence of any Cu complexes indicated that no deactivations occurred due to the absence of deactivators.

Finally, ATRP using *ht*-PLP_{PAN} was extended to other monomers and solvents (**Supplementary Table 1**). For example, methyl acrylate (MA) was polymerized using 100 ppm of the $CuBr_2$/TPMA complex and ethyl α-bromoisobutyrate (EBiB) as the initiator (entry 1, **Supplementary Table 1**). Good control over the polymerization was illustrated by the low $Đ$ = 1.16 of the polymer (**Supplementary Figures 6A,B**). Additionally, ATRP of MMA was performed using 100 ppm of the $CuBr_2$/TPMA complex and anisole as a less polar solvent (entry 2, **Supplementary Table 1**). The rate of polymerization was slower in anisole compared to DMSO/DMF, as expected from the variation of the ATRP equilibrium constant, K_{ATRP}, with solvent polarity (Ribelli et al., 2019). Nonetheless, well-controlled polymerization ($Đ$ = 1.19) was still observed (**Supplementary Figures 6C,D**).

Photocatalytic Mechanism and Comparison Between Activation by Cu^I Complex and by *ht*-PLP_{PAN}

In some ATRP methods with regeneration of the Cu^I/L activator, the agent used for the activator regeneration can also contribute

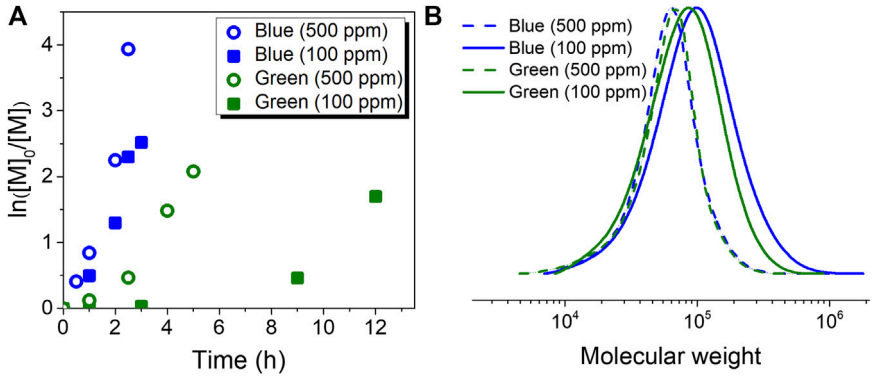

FIGURE 2 | Photoinduced ATRP in water **(A)** First-order kinetic plots corresponding to entries 1 (blue, 500 ppm), 2 (blue, 100 ppm), 6 (green, 500 ppm) and 7 (green, 100 ppm) of **Table 1 (B)** GPC traces corresponding to the polymer product of entries 1, 2, 6 and 7 of **Table 1**.

TABLE 2 | Cu-catalyzed light-mediated ATRP of MMA in DMSO/DMF[a] with EBPA as the initiator and *ht*-PLP_{PAN} as the photo-cocatalyst (0.95 mg/ml).

Entry	Irradiation	$[M]_0/[I]_0/[CuBr_2]_0/[TPMA]_0$	Conv. (%)	$M_{n,theo}$[b]	$M_{n,GPC}$[c]	$Đ$
1	Blue (450 nm)[d]	200/1/0.02/0.06	70 (28 h)	14,200	11,900	1.19
2		200/1/0.005/0.015	63 (25 h)	12,900	9,900	1.60
3		200/1/0/0	49 (12 h)	10,100	120,000	1.92
4		200/0/0/0	<5 (15 h)	–[e]	–	–
5	Green (520 nm)[f]	200/1/0.02/0.06	66 (24 h)	13,400	13,800	1.30
6		200/1/0.005/0.015	40 (25 h)	8,400	8,300	1.41
7		200/1/0/0	<5 (12 h)	–	–	–

[a]*General conditions: Vol%(MMA) = 25% and DMSO/DMF (vol ratio = 1/1) was used as the solvent.* $M_{n,GPC}$ *was calculated from PMMA calibrations.*
[b]$M_{n,theo}$ *was determined by the monomer conversion monitored by* ^1H *NMR.*
[c]$M_{n,GPC}$ *was calculated from a linear PMMA calibration.*
[d]*Intensity: 5.0 mW* cm^{-2}.
[e]*No polymerization was observed on GPC.*
[f]*Intensity: 4.7 mW* cm^{-2}.

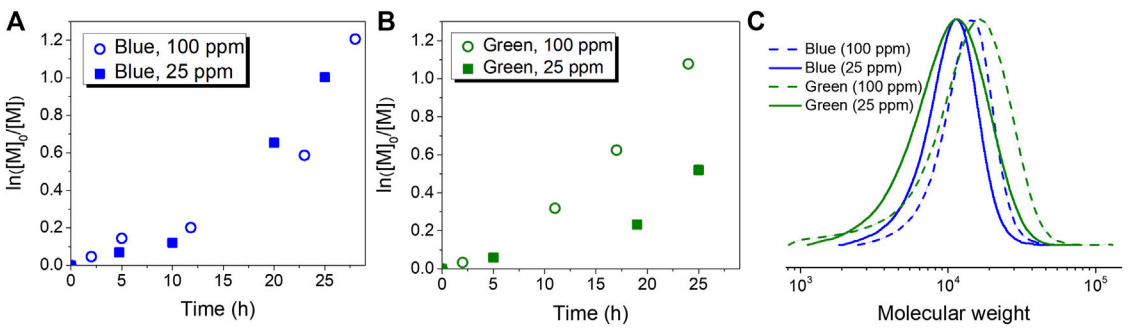

FIGURE 3 | Photoinduced ATRP in organic solvents. First-order kinetic plots corresponding to **(A)** entries 1 (blue, 100 ppm) and 2 (blue, 25 ppm) **(B)** entries 5 (green, 100 ppm) and 6 (green, 25 ppm) of **Table 2**. **(C)** GPC traces corresponding to the polymer product of entries 1, 2, 5 and 6 of **Table 2**.

to the activation of dormant alkyl bromides to form propagating radicals, which generally occurs by reaction between the agent and the alkyl bromide (Konkolewicz et al., 2013; Konkolewicz et al., 2014a; Konkolewicz et al., 2014b; Zhang et al., 2011). To better understand the polymerization mechanism of the current system, the photoreduction of the Cu^{II} complex by *ht*-PLP_{PAN} was first monitored by linear sweep voltammetry (LSV). As shown in **Figure 4**, LSV was scanned from ca. 0.5 V (vs SCE) where the Cu^{I} complex is oxidized if it exists. Indeed, the increased intensity of the anodic current under blue or green

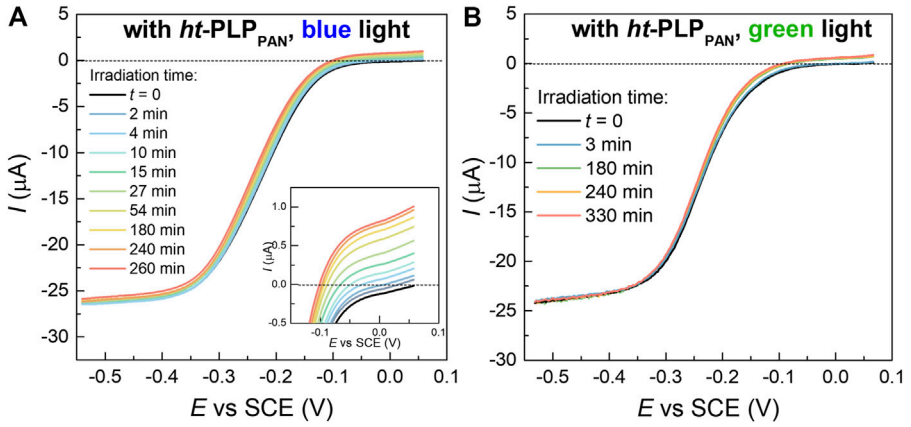

FIGURE 4 | LSV of 0.6 mM $CuBr_2$/TPMA (L/Cu = 3) in DMSO-DMF (volume ratio: 1/1) + 0.1 M Et_4NBF_4 at v = 0.01 $V.s^{-1}$ and RDE rotation speed 4,000 rpm, under **(A)** blue light and **(B)** green light irradiation, in the presence of *ht*-PLP_{PAN} (1.5 mg/ml).

light irradiation confirmed the formation of Cu^I/TPMA complex in DMSO/DMF (volume ratio: 1/1) (Dadashi-Silab et al., 2021). The role of *ht*-PLP_{PAN} as the primary factor behind the observed reduction of Cu^{II}/TPMA complexes after 3 h of blue light irradiation was confirmed by comparing the fraction of Cu^I complexes estimated from the current values in the presence of *ht*-PLP_{PAN} (ca. 2.5%) and in its absence (<0.5%, **Supplementary Figure 7A**). The small extent of photoreduction in the latter case was likely caused by the presence of excess ligand that can act as the electron donor. Notably, the LSV traces acquired in water did not show a consistent increase of Cu^I/L concentration (**Supplementary Figure 7B**), in contrast with polymerization results (**Table 1**) that indicated *ht*-PLP_{PAN} was capable of photoreducing the Cu^{II} complex in water. This apparent discrepancy indicates that the amount of Cu^I produced by *ht*-PLP_{PAN} in water was below the reliable LSV detectability threshold but was still sufficient to effectively initiate polymerization owing to the higher K_{ATRP} of Cu catalysts in water (Tang et al., 2008; Fantin et al., 2015). It should be pointed out that the apparent lower reducing efficiency of *ht*-PLP_{PAN} in water in comparison with organic solvents could be caused by its nano-assembly, which, while important for allowing these mostly hydrophobic species to function in water, would inevitably decrease the number of accessible photocatalytic sites.

To further understand the composition of the catalytic system for aqueous ATRP under blue light irradiation, the following calculations were performed to quantify the concentrations of Cu^I and Cu^{II} species in polymerizations corresponding to conditions in **Table 1**. The activation rates of alkyl bromides by Cu^I/L and *ht*-PLP_{PAN} were estimated for the polymerization of OEGMA (entries 1, 2 and 4 of **Table 1**). First, the rate of activation by the Cu^I complex (R_{a1}) was given by **Eq. (1)**, (Matyjaszewski 2012; Krys et al. 2016; Krys and Matyjaszewski 2017) thus the concentration of the Cu^I complex ([Cu^I/L]) was calculated. **Eq. 2** shows the relationship between [Cu^I/L] and the rate of polymerization, R_p:

$$R_{a1} = k_{a1}[Cu^I/L][RX] \quad (1)$$

$$R_p = k_p K_{ATRP} \frac{[RX][Cu^I/L]}{[Br - Cu^{II}/L]}[M] \quad (2)$$

where, [RX], [M], [Cu^I/L] and [Br-Cu^{II}/L] correspond to the concentration of the alkyl bromide initiator, monomer, Cu^I complex and Cu^{II} complex, respectively. k_{a1} is the activation rate constant of HO-EBiB by Cu^I/TPMA. K_{ATRP} is the ATRP equilibrium constant for Cu^I/TPMA with HO-EBiB, and k_p is the rate coefficient of propagation for OEGMA. (Smolne et al., 2016)

On the other hand, the activation rate of alkyl bromides by *ht*-PLP_{PAN} (R_{a-pc}) was determined from **Eq. 3**:

$$R_{p,\ without\ Cu} = k_p[M][R] = k_p[M]\sqrt{\frac{R_{a-pc}}{k_t}} \quad (3)$$

where, $R_{p,\ without\ Cu}$ refers to the rate of polymerization in the absence of Cu^{II} complex. k_t is the termination rate constant of OEGMA, (Smolne et al., 2016) and [R·] is the concentration of propagating radicals.

Details of the calculation, including the scaling of kinetic parameters, are included in the **Supplementary Material** (**Supplementary Tables 2–4**) (Fantin et al., 2015; Fantin et al., 2017). Specifically, $R_{p,\ without\ Cu}$ was monitored by ^1H NMR (entry 4 of **Table 1**, **Supplementary Figure 8**). The polymerization was slower when no Cu complex was present, and polymers with high molecular weight (over seven times higher than $M_{n,theo}$) were observed by GPC, indicating a low initiation efficiency when *ht*-PLP_{PAN} was the only activator.

As shown in **Table 3**, the calculated $R_{p,\ without\ Cu}$ was 6.34 × 10^{-6} $M.s^{-1}$, which was ca. one order of magnitude smaller than R_p[R_p (100 ppm) = 5.46 × 10^{-5} $M.s^{-1}$, R_p (500 ppm) = 7.22 × 10^{-5} $M.s^{-1}$]. Based on these values, the calculated [Cu^I/L] was 5.5 × 10^{-7} M for ATRP using 100 ppm of $CuBr_2$/TPMA, and

TABLE 3 | Calculated reaction parameters during light-mediated ATRP of OEGMA catalyzed by $CuBr_2$/TPMA. Total concentrations for Cu species were 0.054 mM (entry 1, **Table 1**) and 0.27 mM (entry 2, **Table 1**), respectively. The concentration of HO-EBiB was 2.7 mM in both entries.

Entry	Loading of Cu complex (ppm)	R_p[a]	[Cu^I/L]	Cu^I/L %[b] (%)	R_{a1}[c]
1	100	5.46×10^{-5} M.s^{-1}	5.5×10^{-7} M	1.0	8.1×10^{-5} M.s^{-1}
2	500	7.22×10^{-5} M.s^{-1}	3.6×10^{-6} M	1.4	5.3×10^{-4} M.s^{-1}

[a]*Rate of polymerization.*

[b]*Molar fraction of Cu^I/L complex during the polymerization.*

[c]*Activation rate of R-Br by Cu^I/L complex. In comparison, the estimated activation rate of R-Br by* ht-PLP_{PAN} *(in the absence of Cu species) was 9.3×10^{-10} M.s^{-1}. See* ***Supplementary Material*** *for calculation methods.*

3.6×10^{-6} M for ATRP using 500 ppm of $CuBr_2$/TPMA. Although Cu^I/L only consisted of 1.0% (entry 1, **Table 3**) and 1.4 (entry 2, **Table 3**) of the total Cu species, the calculated values of R_{a1} (**Table 3**) were five to six orders of magnitude higher than R_{a-pc} (9.3×10^{-10} M.s^{-1}). This significant difference in the activation rate was due to the high k_{a1} value of [Cu^I/TPMA]$^+$ in aqueous media (Fantin et al., 2017), making Cu^I/L the predominant activator over *ht*-PLP_{PAN} in this system.

CONCLUSIONS AND PERSPECTIVES

In conclusion, a dispersible PAN-derived photo-cocatalyst, *ht*-PLP_{PAN}, was applied as OPCs in Cu-catalyzed ATRP under blue or green light irradiation. Hydrophilic and hydrophobic functional groups prompted *ht*-PLP_{PAN} to assemble into spherical OPNOs in water. Compared to previously reported photoinduced CRPs using self-assembled photocatalysts, this work expanded the utilization of OPNO-based photocatalysts or photo-cocatalysts from organic solvents (DMF/DMSO, anisole) to aqueous media. Well-controlled polymerization of acrylate and methacrylate monomers were reported. Furthermore, analysis of the R-Br activation demonstrated how the irradiation wavelength affected the activation mechanism of Cu-catalyzed ATRP. Control experiments showed that both *ht*-PLP_{PAN} and the Cu^I complex could activate R-Br under blue light irradiation. While under green light irradiation, the Cu^I complex was the only activator for R-Br. But the reaction between the Cu^I complex and R-Br was five to six orders of magnitude faster than the activation of R-Br by *ht*-PLP_{PAN}, due to the high activation rate constant of the Cu^I complex, particularly in aqueous media.

DATA AVAILABILITY STATEMENT

The original contributions presented in the study are included in the article/**Supplementary Material**, further inquiries can be directed to the corresponding author.

AUTHOR CONTRIBUTIONS

MS designed and performed the experiments. FL designed and performed the voltammetric analysis. RY prepared the polymer substrate. MS, FL, SD-S, TK and KM discussed the photocatalytic mechanism. TK performed the DFT calculations. All authors contributed to the preparation and revision of the manuscript.

FUNDING

Financial support from the Department of Energy (ER45998) is greatly appreciated.

ACKNOWLEDGMENTS

The authors acknowledge use of the Materials Characterization Facility at Carnegie Mellon University supported by grant MCF-677785.

SUPPLEMENTARY MATERIAL

The Supplementary Material for this article can be found online at: https://www.frontiersin.org/articles/10.3389/fchem.2021.734076/full#supplementary-material

REFERENCES

Allegrezza, M. L., and Konkolewicz, D. (2021). PET-RAFT Polymerization: Mechanistic Perspectives for Future Materials. *ACS Macro Lett.* 10, 433–446. doi:10.1021/acsmacrolett.1c00046

Cao, S., Le, A. N., Chen, A., and Zhong, M. (2020). Scalable Synthesis of Fluorescent Organic Nanodots by Block Copolymer Templating. *J. Polym. Sci.* 58, 30–34. doi:10.1002/pola.2946610.1002/pol.20190265

Chai, J.-D., and Head-Gordon, M. (2008). Long-range Corrected Hybrid Density Functionals with Damped Atom-Atom Dispersion Corrections. *Phys. Chem. Chem. Phys.* 10, 6615–6620. doi:10.1039/B810189B

Chen, M., Zhong, M., and Johnson, J. A. (2016). Light-Controlled Radical Polymerization: Mechanisms, Methods, and Applications. *Chem. Rev.* 116, 10167–10211. doi:10.1021/acs.chemrev.5b00671

Chen, T.-H., and Tseng, W.-L. (2017). Self-Assembly of Monodisperse Carbon Dots into High-Brightness Nanoaggregates for Cellular Uptake Imaging and Iron(III) Sensing. *Anal. Chem.* 89, 11348–11356. doi:10.1021/acs.analchem.7b02193

Chmielarz, P., Fantin, M., Park, S., Isse, A. A., Gennaro, A., Magenau, A. J. D., et al. (2017). Electrochemically Mediated Atom Transfer Radical Polymerization (eATRP). *Prog. Polym. Sci.* 69, 47–78. doi:10.1016/j.progpolymsci.2017.02.005

Corrigan, N., Jung, K., Moad, G., Hawker, C. J., Matyjaszewski, K., and Boyer, C. (2020). Reversible-deactivation Radical Polymerization (Controlled/living Radical

Polymerization): From Discovery to Materials Design and Applications. *Prog. Polym. Sci.* 111, 101311. doi:10.1016/j.progpolymsci.2020.101311

Dadashi-Silab, S., Atilla Tasdelen, M., and Yagci, Y. (2014). Photoinitiated Atom Transfer Radical Polymerization: Current Status and Future Perspectives. *J. Polym. Sci. Part. A: Polym. Chem.* 52, 2878–2888. doi:10.1002/pola.27327

Dadashi-Silab, S., Doran, S., and Yagci, Y. (2016). Photoinduced Electron Transfer Reactions for Macromolecular Syntheses. *Chem. Rev.* 116, 10212–10275. doi:10.1021/acs.chemrev.5b00586

Dadashi-Silab, S., Lorandi, F., DiTucci, M. J., Sun, M., Szczepaniak, G., Liu, T., et al. (2021). Conjugated Cross-Linked Phenothiazines as Green or Red Light Heterogeneous Photocatalysts for Copper-Catalyzed Atom Transfer Radical Polymerization *J. Am. Chem. Soc.* 143, 9630–9638. doi:10.1021/jacs.1c04428

El Achi, N., Bakkour, Y., Adhami, W., Molina, J., Penhoat, M., Azaroual, N., et al. (2020). Metal-Free ATRP Catalyzed by Visible Light in Continuous Flow. *Front. Chem.* 8, 740. doi:10.3389/fchem.2020.00740

Ermakov, I. V., Rebrov, A. I., Litmanovich, A. D., and Platé, N. A. (2000). Alkaline Hydrolysis of Polyacrylonitrile, 1. Structure of the Reaction Products. *Macromol. Chem. Phys.* 201, 1415–1418. doi:10.1002/1521-3935(20000801)201:13<1415::AID-MACP1415>3.0.CO;2-R

Fantin, M., Isse, A. A., Gennaro, A., and Matyjaszewski, K. (2015). Understanding the Fundamentals of Aqueous ATRP and Defining Conditions for Better Control. *Macromolecules* 48, 6862–6875. doi:10.1021/acs.macromol.5b01454

Fantin, M., Isse, A. A., Matyjaszewski, K., and Gennaro, A. (2017). ATRP in Water: Kinetic Analysis of Active and Super-active Catalysts for Enhanced Polymerization Control. *Macromolecules* 50, 2696–2705. doi:10.1021/acs.macromol.7b00246

Frisch, M. J., Trucks, G. W., Schlegel, H. B., Scuseria, G. E., Robb, M. A., Cheeseman, J. R., et al. (2016). *Gaussian 09*. Wallingford, CT: Rev. A.02.

Fu, L., Simakova, A., Fantin, M., Wang, Y., and Matyjaszewski, K. (2018). Direct ATRP of Methacrylic Acid with Iron-Porphyrin Based Catalysts. *ACS Macro Lett.* 7, 26–30. doi:10.1021/acsmacrolett.7b00909

Go, D., Jurásková, A., Hoffmann, A., Kapiti, G., and Kuehne, A. J. C. (2017). Deep-Blue Fluorescent Particles via Microwave Heating of Polyacrylonitrile Dispersions. *Macromol. Rapid Commun.* 38, 1600775. doi:10.1002/marc.201600775

Gottlieb, E., Matyjaszewski, K., and Kowalewski, T. (2019). Polymer-Based Synthetic Routes to Carbon-Based Metal-Free Catalysts. *Adv. Mater.* 31, 1804626. doi:10.1002/adma.201804626

Han, M., Zhu, S., Lu, S., Song, Y., Feng, T., Tao, S., et al. (2018). Recent Progress on the Photocatalysis of Carbon Dots: Classification, Mechanism and Applications. *Nano Today* 19, 201–218. doi:10.1016/j.nantod.2018.02.008

Hao, Q., Qiao, L., Shi, G., He, Y., Cui, Z., Fu, P., et al. (2021). Effect of Nitrogen Type on Carbon Dot Photocatalysts for Visible-Light-Induced Atom Transfer Radical Polymerization. *Polym. Chem.* 12, 3060–3066. doi:10.1039/D1PY00148E

Jang, J., Bae, J., and Park, E. (2006). Polyacrylonitrile Nanofibers: Formation Mechanism and Applications as a Photoluminescent Material and Carbon-Nanofiber Precursor. *Adv. Funct. Mater.* 16, 1400–1406. doi:10.1002/adfm.200500598

Jia, Q., Ge, J., Liu, W., Guo, L., Zheng, X., Chen, S., et al. (2017). Self-Assembled Carbon Dot Nanosphere: A Robust, Near-Infrared Light-Responsive, and Vein Injectable Photosensitizer. *Adv. Healthc. Mater.* 6, 1601419. doi:10.1002/adhm.201601419

Jiang, J., Ye, G., Wang, Z., Lu, Y., Chen, J., and Matyjaszewski, K. (2018). Heteroatom-Doped Carbon Dots (CDs) as a Class of Metal-Free Photocatalysts for PET-RAFT Polymerization under Visible Light and Sunlight. *Angew. Chem. Int. Ed.* 57, 12037–12042. doi:10.1002/anie.201807385

Konkolewicz, D., Krys, P., Góis, J. R., Mendonça, P. V., Zhong, M., Wang, Y., et al. (2014). Aqueous RDRP in the Presence of Cu0: The Exceptional Activity of CuI Confirms the SARA ATRP Mechanism. *Macromolecules* 47, 560–570. doi:10.1021/ma4022983

Konkolewicz, D., Schröder, K., Buback, J., Bernhard, S., and Matyjaszewski, K. (2012). Visible Light and Sunlight Photoinduced ATRP with Ppm of Cu Catalyst. *ACS Macro Lett.* 1, 1219–1223. doi:10.1021/mz300457e

Konkolewicz, D., Wang, Y., Krys, P., Zhong, M., Isse, A. A., Gennaro, A., et al. (2014). SARA ATRP or SET-LRP. End of Controversy? *Polym. Chem.* 5, 4409–4417. doi:10.1039/C4PY00149D

Konkolewicz, D., Wang, Y., Zhong, M., Krys, P., Isse, A. A., Gennaro, A., et al. (2013). Reversible-Deactivation Radical Polymerization in the Presence of Metallic Copper. A Critical Assessment of the SARA ATRP and SET-LRP Mechanisms. *Macromolecules* 46, 8749–8772. doi:10.1021/ma401243k

Kopeć, M., Lamson, M., Yuan, R., Tang, C., Kruk, M., Zhong, M., et al. (2019). Polyacrylonitrile-derived Nanostructured Carbon Materials. *Prog. Polym. Sci.* 92, 89–134. doi:10.1016/j.progpolymsci.2019.02.003

Kopeć, M., Pikiel, M., and Vancso, G. J. (2020). Surface-grafted Polyacrylonitrile Brushes with Aggregation-Induced Emission Properties. *Polym. Chem.* 11, 669–674. doi:10.1039/C9PY01213C

Kopeć, M., Yuan, R., Gottlieb, E., Abreu, C. M. R., Song, Y., Wang, Z., et al. (2017). Polyacrylonitrile-b-poly(butyl Acrylate) Block Copolymers as Precursors to Mesoporous Nitrogen-Doped Carbons: Synthesis and Nanostructure. *Macromolecules* 50, 2759–2767. doi:10.1021/acs.macromol.6b02678

Krys, P., and Matyjaszewski, K. (2017). Kinetics of Atom Transfer Radical Polymerization. *Eur. Polym. J.* 89, 482–523. doi:10.1016/j.eurpolymj.2017.02.034

Krys, P., Ribelli, T. G., Matyjaszewski, K., and Gennaro, A. (2016). Relation between Overall Rate of ATRP and Rates of Activation of Dormant Species. *Macromolecules* 49, 2467–2476. doi:10.1021/acs.macromol.6b00058

Kutahya, C., Aykac, F. S., Yilmaz, G., and Yagci, Y. (2016). LED and Visible Light-Induced Metal Free ATRP Using Reducible Dyes in the Presence of Amines. *Polym. Chem.* 7, 6094–6098. doi:10.1039/C6PY01417H

Kütahya, C., Wang, P., Li, S., Liu, S., Li, J., Chen, Z., et al. (2020). Carbon Dots as a Promising Green Photocatalyst for Free Radical and ATRP-Based Radical Photopolymerization with Blue LEDs. *Angew. Chem. Int. Ed.* 59, 3166–3171. doi:10.1002/anie.201912343

Kütahya, C., Zhai, Y., Li, S., Liu, S., Li, J., Strehmel, V., et al. (2021). Distinct Sustainable Carbon Nanodots Enable Free Radical Photopolymerization, Photo-ATRP and Photo-CuAAC Chemistry. *Angew. Chem. Int. Ed.* 60, 10983–10991. doi:10.1002/anie.202015677

Lamson, M., Kopeć, M., Ding, H., Zhong, M., and Matyjaszewski, K. (2016). Synthesis of Well-Defined Polyacrylonitrile by ICARATRP with Low Concentrations of Catalyst. *J. Polym. Sci. Part. A: Polym. Chem.* 54, 1961–1968. doi:10.1002/pola.28055

Lorandi, F., and Matyjaszewski, K. (2020). Why Do We Need More Active ATRP Catalysts?. *Isr. J. Chem.* 60, 108–123. doi:10.1002/ijch.201900079

Matyjaszewski, K. (2018). Advanced Materials by Atom Transfer Radical Polymerization. *Adv. Mater.* 30, 1706441. doi:10.1002/adma.201706441

Matyjaszewski, K. (2012). Atom Transfer Radical Polymerization (ATRP): Current Status and Future Perspectives. *Macromolecules* 45, 4015–4039. doi:10.1021/ma3001719

Matyjaszewski, K., and Tsarevsky, N. V. (2014). Macromolecular Engineering by Atom Transfer Radical Polymerization. *J. Am. Chem. Soc.* 136, 6513–6533. doi:10.1021/ja408069v

Matyjaszewski, K., and Xia, J. (2001). Atom Transfer Radical Polymerization. *Chem. Rev.* 101, 2921–2990. doi:10.1021/cr940534g

Melchionna, M., and Fornasiero, P. (2020). Updates on the Roadmap for Photocatalysis. *ACS Catal.* 10, 5493–5501. doi:10.1021/acscatal.0c01204

Mendonça, P. V., Averick, S. E., Konkolewicz, D., Serra, A. C., Popov, A. V., Guliashvili, T., et al. (2014). Straightforward ARGET ATRP for the Synthesis of Primary Amine Polymethacrylate with Improved Chain-End Functionality under Mild Reaction Conditions. *Macromolecules* 47, 4615–4621. doi:10.1021/ma501007j

Miertuš, S. S., and Tomasi, J. (1981). Electrostatic Interaction of a Solute with a Continuum. A Direct Utilizaion of Ab Initio Molecular Potentials for the Prevision of Solvent Effects. *Chem. Phys.* 55, 117–129. doi:10.1016/0301-0104(81)85090-2

Mohapatra, H., Kleiman, M., and Esser-Kahn, A. P. (2017). Mechanically Controlled Radical Polymerization Initiated by Ultrasound. *Nat. Chem* 9, 135–139. doi:10.1038/nchem.2633

Pan, X., Fang, C., Fantin, M., Malhotra, N., So, W. Y., Peteanu, L. A., et al. (2016). Mechanism of Photoinduced Metal-free Atom Transfer Radical Polymerization: Experimental and Computational Studies. *J. Am. Chem. Soc.* 138, 2411–2425. doi:10.1021/jacs.5b13455

Pan, X., Fantin, M., Yuan, F., and Matyjaszewski, K. (2018). Externally Controlled Atom Transfer Radical Polymerization. *Chem. Soc. Rev.* 47, 5457–5490. doi:10.1039/C8CS00259B

Pan, X., Malhotra, N., Simakova, A., Wang, Z., Konkolewicz, D., and Matyjaszewski, K. (2015). Photoinduced Atom Transfer Radical Polymerization with Ppm-Level Cu Catalyst by Visible Light in Aqueous Media. *J. Am. Chem. Soc.* 137, 15430–15433. doi:10.1021/jacs.5b11599

Pan, X., Tasdelen, M. A., Laun, J., Junkers, T., Yagci, Y., and Matyjaszewski, K. (2016). Photomediated Controlled Radical Polymerization. *Prog. Polym. Sci.* 62, 73–125. doi:10.1016/j.progpolymsci.2016.06.005

Parkatzidis, K., Wang, H. S., Truong, N. P., and Anastasaki, A. (2020). Recent Developments and Future Challenges in Controlled Radical Polymerization: A 2020 Update. *Chem.* 6, 1575–1588. doi:10.1016/j.chempr.2020.06.014

Pearson, R. M., Lim, C.-H., McCarthy, B. G., Musgrave, C. B., and Miyake, G. M. (2016). Organocatalyzed Atom Transfer Radical Polymerization Using N-Aryl Phenoxazines as Photoredox Catalysts. *J. Am. Chem. Soc.* 138, 11399–11407. doi:10.1021/jacs.6b08068

Perrier, S. (2017). 50th Anniversary Perspective: RAFT Polymerization-A User Guide. *Macromolecules* 50, 7433–7447. doi:10.1021/acs.macromol.7b00767

Ribelli, T. G., Lorandi, F., Fantin, M., and Matyjaszewski, K. (2019). Atom Transfer Radical Polymerization: Billion Times More Active Catalysts and New Initiation Systems. *Macromol. Rapid Commun.* 40, 1800616. doi:10.1002/marc.201800616

Romero, N. A., and Nicewicz, D. A. (2016). Organic Photoredox Catalysis. *Chem. Rev.* 116, 10075–10166. doi:10.1021/acs.chemrev.6b00057

Simakova, A., Averick, S. E., Konkolewicz, D., and Matyjaszewski, K. (2012). Aqueous ARGET ATRP. *Macromolecules* 45, 6371–6379. doi:10.1021/ma301303b

Smolne, S., Weber, S., and Buback, M. (2016). Propagation and Termination Kinetics of Poly(Ethylene Glycol) Methyl Ether Methacrylate in Aqueous Solution. *Macromol. Chem. Phys.* 217, 2391–2401. doi:10.1002/macp.201600302

Stephens, P. J., Devlin, F. J., Chabalowski, C. F., and Frisch, M. J. (1994). Ab Initio Calculation of Vibrational Absorption and Circular Dichroism Spectra Using Density Functional Force Fields. *J. Phys. Chem.* 98, 11623–11627. doi:10.1021/j100096a001

Sun, M., Gottlieb, E., Yuan, R., Ghosh, S., Wang, H., Selhorst, R., et al. (2020). Polyene-Free Photoluminescent Polymers via Hydrothermal Hydrolysis of Polyacrylonitrile in Neutral Water. *ACS Macro Lett.* 9, 1403–1408. doi:10.1021/acsmacrolett.0c00410

Sun, Y.-P., Zhou, B., Lin, Y., Wang, W., Fernando, K. A. S., Pathak, P., et al. (2006). Quantum-sized Carbon Dots for Bright and Colorful Photoluminescence. *J. Am. Chem. Soc.* 128, 7756–7757. doi:10.1021/ja062677d

Szczepaniak, G., Łagodzińska, M., Dadashi-Silab, S., Gorczyński, A., and Matyjaszewski, K. (2020). Fully Oxygen-Tolerant Atom Transfer Radical Polymerization Triggered by Sodium Pyruvate. *Chem. Sci.* 11, 8809–8816. doi:10.1039/D0SC03179H

Tang, C., Tracz, A., Kruk, M., Zhang, R., Smilgies, D.-M., Matyjaszewski, K., et al. (2005). Long-range Ordered Thin Films of Block Copolymers Prepared by Zone-Casting and Their thermal Conversion into Ordered Nanostructured Carbon. *J. Am. Chem. Soc.* 127, 6918–6919. doi:10.1021/ja0508929

Tang, W., Kwak, Y., Braunecker, W., Tsarevsky, N. V., Coote, M. L., and Matyjaszewski, K. (2008). Understanding Atom Transfer Radical Polymerization: Effect of Ligand and Initiator Structures on the Equilibrium Constants. *J. Am. Chem. Soc.* 130, 10702–10713. doi:10.1021/ja802290a

Tao, S., Feng, T., Zheng, C., Zhu, S., and Yang, B. (2019). Carbonized Polymer Dots: A Brand New Perspective to Recognize Luminescent Carbon-Based Nanomaterials. *J. Phys. Chem. Lett.* 10, 5182–5188. doi:10.1021/acs.jpclett.9b01384

Theriot, J. C., Lim, C.-H., Yang, H., Ryan, M. D., Musgrave, C. B., and Miyake, G. M. (2016). Organocatalyzed Atom Transfer Radical Polymerization Driven by Visible Light. *Science* 352, 1082–1086. doi:10.1126/science.aaf3935

Treat, N. J., Sprafke, H., Kramer, J. W., Clark, P. G., Barton, B. E., Read de Alaniz, J., et al. (2014). Metal-Free Atom Transfer Radical Polymerization. *J. Am. Chem. Soc.* 136, 16096–16101. doi:10.1021/ja510389m

Wang, J.-S., and Matyjaszewski, K. (1995). Controlled/"living" Radical Polymerization. Atom Transfer Radical Polymerization in the Presence of Transition-Metal Complexes. *J. Am. Chem. Soc.* 117, 5614–5615. doi:10.1021/ja00125a035

Wang, Z., Pan, X., Li, L., Fantin, M., Yan, J., Wang, Z., et al. (2017). Enhancing Mechanically Induced ATRP by Promoting Interfacial Electron Transfer from Piezoelectric Nanoparticles to Cu Catalysts. *Macromolecules* 50, 7940–7948. doi:10.1021/acs.macromol.7b01597

Wu, C., Corrigan, N., Lim, C.-H., Jung, K., Zhu, J., Miyake, G., et al. (2019). Guiding the Design of Organic Photocatalyst for PET-RAFT Polymerization: Halogenated Xanthene Dyes. *Macromolecules* 52, 236–248. doi:10.1021/acs.macromol.8b02517

Xia, C., Zhu, S., Feng, T., Yang, M., and Yang, B. (2019). Evolution and Synthesis of Carbon Dots: From Carbon Dots to Carbonized Polymer Dots. *Adv. Sci.* 6, 1901316. doi:10.1002/advs.201901316

Xia, J., and Matyjaszewski, K. (1999). Controlled/"Living" Radical Polymerization. Atom Transfer Radical Polymerization Catalyzed by Copper(I) and Picolylamine Complexes. *Macromolecules* 32, 2434–2437. doi:10.1021/ma981694n

Xu, J., Shanmugam, S., Duong, H. T., and Boyer, C. (2015). Organo-photocatalysts for Photoinduced Electron Transfer-Reversible Addition-Fragmentation Chain Transfer (PET-RAFT) Polymerization. *Polym. Chem.* 6, 5615–5624. doi:10.1039/C4PY01317D

Yuan, R., Wang, H., Sun, M., Damodaran, K., Gottlieb, E., Kopeć, M., et al. (2019). Well-Defined N/S Co-doped Nanocarbons from Sulfurized PAN-B-PBA Block Copolymers: Structure and Supercapacitor Performance. *ACS Appl. Nano Mater.* 2, 2467–2474. doi:10.1021/acsanm.9b00340

Yuan, R., Wang, H., Sun, M., Whitacre, J., Matyjaszewski, K., and Kowalewski, T. (2020). Copolymer-Derived N/B Co-Doped Nanocarbons with Controlled Porosity and Highly Active Surface. *J. Polym. Sci.* 58, 225–232. doi:10.1002/pol.20190002

Zhang, Y., Wang, Y., and Matyjaszewski, K. (2011). ATRP of Methyl Acrylate with Metallic Zinc, Magnesium, and Iron as Reducing Agents and Supplemental Activators. *Macromolecules* 44, 683–685. doi:10.1021/ma102492c

Zhang, Z., Yi, G., Li, P., Zhang, X., Fan, H., Zhang, Y., et al. (2020). A Minireview on Doped Carbon Dots for Photocatalytic and Electrocatalytic Applications. *Nanoscale* 12, 13899–13906. doi:10.1039/D0NR03163A

Zhao, P., Wang, L., Wu, Y., Yang, T., Ding, Y., Yang, H. G., et al. (2019). Hyperbranched Conjugated Polymer Dots: The Enhanced Photocatalytic Activity for Visible Light-Driven Hydrogen Production. *Macromolecules* 52, 4376–4384. doi:10.1021/acs.macromol.9b00551

Zhong, M., Kim, E. K., McGann, J. P., Chun, S.-E., Whitacre, J. F., Jaroniec, M., et al. (2012). Electrochemically Active Nitrogen-Enriched Nanocarbons with Well-Defined Morphology Synthesized by Pyrolysis of Self-Assembled Block Copolymer. *J. Am. Chem. Soc.* 134, 14846–14857. doi:10.1021/ja304352n

Zhou, Q., Cao, B., Zhu, C., Xu, S., Gong, Y., Yuan, W. Z., et al. (2016). Clustering-Triggered Emission of Nonconjugated Polyacrylonitrile. *Small* 12, 6586–6592. doi:10.1002/smll.201601545

Zhu, S., Meng, Q., Wang, L., Zhang, J., Song, Y., Jin, H., et al. (2013). Highly Photoluminescent Carbon Dots for Multicolor Patterning, Sensors, and Bioimaging. *Angew. Chem. Int. Ed.* 52, 3953–3957. doi:10.1002/anie.201300519

Zhu, S., Song, Y., Shao, J., Zhao, X., and Yang, B. (2015). Non-Conjugated Polymer Dots with Crosslink-Enhanced Emission in the Absence of Fluorophore Units. *Angew. Chem. Int. Ed.* 54, 14626–14637. doi:10.1002/anie.201504951

Zhu, S., Song, Y., Zhao, X., Shao, J., Zhang, J., and Yang, B. (2015). The Photoluminescence Mechanism in Carbon Dots (Graphene Quantum Dots, Carbon Nanodots, and Polymer Dots): Current State and Future Perspective. *Nano Res.* 8, 355–381. doi:10.1007/s12274-014-0644-3

Zhu, S., and Wang, D. (2017). Photocatalysis: Basic Principles, Diverse Forms of Implementations and Emerging Scientific Opportunities. *Adv. Energ. Mater.* 7, 1700841. doi:10.1002/aenm.201700841

Conflict of Interest: The authors declare that the research was conducted in the absence of any commercial or financial relationships that could be construed as a potential conflict of interest.

The handling Editor declared a past co-authorship with one of the authors KM.